

Tentative rotation in a galaxy at $z \sim 14$ with ALMA

J. Scholtz^{*1,2} †, E. Parlanti^{‡3,4}, S. Carniani³, M. Kohandel³, F. Sun⁵, A. L. Danhaive^{1,2}, R. Maiolino^{1,2,6}, S. Arribas⁷, R. Bhatawdekar⁸, A. J. Bunker⁹, S. Charlot¹⁰, F. D’Eugenio^{1,2}, A. Ferrara³, Z. Ji¹¹, Gareth C. Jones^{1,2}, P. Rinaldi¹¹, B. Robertson¹², A. Pallottini^{3,13}, I. Shivaeei⁷, Y. Sun¹¹, S. Tacchella^{1,2}, H. Übler⁴, G. Venturi³

¹ *Kavli Institute for Cosmology, University of Cambridge, Madingley Road, Cambridge, CB3 0HA, UK*

² *Cavendish Laboratory, University of Cambridge, 19 JJ Thomson Avenue, Cambridge CB3 0HE, UK*

³ *Scuola Normale Superiore, Piazza dei Cavalieri 7, I-56126 Pisa, Italy*

⁴ *Max-Planck-Institut für extraterrestrische Physik (MPE), Gießenbachstraße 1, 85748 Garching, Germany*

⁵ *Center for Astrophysics | Harvard & Smithsonian, 60 Garden St., Cambridge MA 02138 USA*

⁶ *Department of Physics and Astronomy, University College London, Gower Street, London WC1E 6BT, UK*

⁷ *Centro de Astrobiología (CAB), CSIC-INTA, Cra. de Ajalvir Km. 4, 28850- Torrejón de Ardoz, Madrid, Spain*

⁸ *European Space Agency (ESA), European Space Astronomy Centre (ESAC), Camino Bajo del Castillo s/n, 28692 Villanueva de la Cañada, Madrid, Spain*

⁹ *University of Oxford, Department of Physics, Denys Wilkinson Building, Keble Road, Oxford OX13RH, United Kingdom*

¹⁰ *Sorbonne Université, CNRS, UMR 7095, Institut d’Astrophysique de Paris, 98 bis bd Arago, 75014 Paris, France*

¹¹ *Steward Observatory, University of Arizona, 933 N. Cherry Avenue, Tucson, AZ 85721, USA*

¹² *Department of Astronomy and Astrophysics University of California, Santa Cruz, 1156 High Street, Santa Cruz CA 96054, USA*

¹³ *Dipartimento di Fisica “Enrico Fermi”, Università di Pisa, Largo Bruno Pontecorvo 3, Pisa I-56127, Italy*

Accepted XXX. Received YYY; in original form ZZZ

ABSTRACT

We re-analysed ALMA observations of the [O III] $\lambda 88\mu\text{m}$ emission line in JADES-GS-z14-0, so far the most distant spectroscopically confirmed galaxy at $z=14.18$. Our analysis shows a tentative detection of a velocity gradient of [O III] $\lambda 88\mu\text{m}$ using three independent tests: 1) construction of moment maps; 2) extraction of integrated spectra from a grid of apertures; and 3) spectro-astrometry in both the image and uv planes. We performed kinematical fitting using the KinMS code and estimated a dynamical mass of $\log_{10}(M_{\text{dyn}}/M_{\odot}) = 9.4^{+0.8}_{-0.4}$, with the bulk of the uncertainties due to the degeneracy between dynamical mass and inclination. We measure an upper limit on the velocity dispersion (σ_v) of $< 40 \text{ km s}^{-1}$ which results in an estimate of $V_{\text{rot}}/\sigma > 2.5$. This result, if confirmed with higher-resolution observations, would imply that kinematically cold discs are already in place at $z \sim 14$. Comparison with mock observations from the SERRA cosmological simulations confirms that even low-resolution observations are capable of detecting a velocity gradient in $z > 10$ galaxies as compact as JADES-GS-z14-0. This work shows that deeper ALMA or JWST/NIRSpec IFS observations with high spatial resolution will be able to estimate an accurate dynamical mass for JADES-GS-z14-0, providing an upper limit to the stellar mass of this over-luminous galaxy.

Key words: galaxies; kinematics & dynamics — galaxies: evolution;

1 INTRODUCTION

With the launch of the James Webb Space Telescope (JWST), we are now able to observe the rest-frame optical and UV emission from galaxies and their interstellar medium (ISM) up to redshift ~ 14 (Cameron et al. 2023; Curtis-Lake et al. 2023; Harikane et al. 2023; Larson et al. 2023; Isobe et al. 2023; Hsiao et al. 2023; Robertson et al. 2023; Abdurro’uf et al. 2024; Carniani et al. 2024a; Harikane et al. 2024; Sanders et al. 2024; Tacchella et al. 2023, 2024; Vikaeus et al. 2024), revealing a large population of bright, metal-poor galaxies in the early Universe. However, the most distant galaxy is also de-

tected in interferometric observations in/from line emission (ALMA; Carniani et al. 2024b; Schouws et al. 2024).

Before the launch of JWST, the main avenue to study galaxies properties of high-redshift galaxies was with HST and ground-based 8–10 m observatories to study the rest-frame UV properties. Mm/sub-mm observatories such as ALMA and NOEMA investigated these high- z galaxies through [C II] $\lambda 158\mu\text{m}$ and [O III] $\lambda 88\mu\text{m}$ emission lines and in a few cases far-IR continuum emission. These observations revealed large dust reservoirs by $z \sim 8$ (Tamura et al. 2019; Bakx et al. 2021; Inami et al. 2022; Sommovigo et al. 2022; Witstok et al. 2022), but also ISM properties such as metallicity and ionisation parameter (Spilker et al. 2022; Witstok et al. 2022; Litke et al. 2023; Killi et al. 2023).

Far infra-red (FIR) observations of high- z galaxies also showed early rotating discs (e.g. Smit et al. 2018; Neeleman et al. 2020;

* E-mail: js2685@cam.ac.uk

† These authors contributed to this work equally.

‡ E-mail: eleonora.parlanti@sns.it

Rizzo et al. 2020; Fraternali et al. 2021; Lelli et al. 2021; Rizzo et al. 2021; Parlanti et al. 2023; Rowland et al. 2024). However, in some cases, *JWST* observations have resolved these apparent discs into close-separation major mergers (e.g. Fraternali et al. 2021; Jones et al. 2024; Lamperti et al. 2024; Scholtz et al. 2024; Parlanti et al. 2024; Übler et al. 2024), although there is still debate over different kinematic signatures in cold and ionised gas phases. Theoretical models predict that high redshift galaxies should be more turbulent, due to the increased merger rates (Duncan et al. 2019; Duan et al. 2024), violent disc instabilities driven by the accretion of gas (Dekel et al. 2009; Krumholz et al. 2018), and intense star formation feedback (Orr et al. 2020). However, different cosmological simulations find different results, with some showing the presence of turbulent discs (Pillepich et al. 2019), while others predict that early galaxies should already have formed a cold rotating disc (Kohandel et al. 2024). This still leaves major questions about the assembly of discs at the epoch of reionisation and beyond, including which gas phase best traces the galaxy kinematics/rotation.

The most distant spectroscopically confirmed galaxy is JADES-GS-53.08294-27.85563 (more commonly known as JADES-GS-z14-0; Robertson et al. 2024) at $z = 14.1796$, originally identified via NIRC*am* photometry (Hainline et al. 2024; Robertson et al. 2024) and later spectroscopically confirmed by NIRS*pec* (Carniani et al. 2024a), and ALMA (Carniani et al. 2024b; Schouws et al. 2024). The combination of ALMA and *JWST* observations revealed a compact galaxy with a size of 260 ± 20 pc with metallicity of $0.1-0.2 Z_{\odot}$, i.e. a significantly enriched ISM for $z \sim 14$ galaxy (Carniani et al. 2024a). The galaxy is also detected at $7.7 \mu\text{m}$ with MIRI with strong excess to NIRC*am* photometry, indicating the presence of $[\text{O III}]\lambda\lambda 5007, 4959$ (Helton et al. 2024). Furthermore, Carniani et al. (2024b) and Schouws et al. (2024) detected $[\text{O III}]\lambda 88 \mu\text{m}$ in this galaxy with ALMA, measuring the dynamical mass from the velocity dispersion of the $[\text{O III}]\lambda 88 \mu\text{m}$ ($\log_{10}(M_{\text{dyn}}/M_{\odot}) = 9.0 \pm 0.2$), comparable to the galaxy’s stellar mass ($\log_{10}(M_{*}/M_{\odot}) = 8.7^{+0.7}_{-0.2}$). Under standard assumptions about stellar-population modelling (e.g., Chabrier 2003 initial mass function; Carniani et al. 2024b; Helton et al. 2024), the measured dynamical mass leaves very little mass budget for both gas and stars – the estimated gas fraction is only 10–30 %, making this galaxy gas-poor. This would be a result of either rapid gas consumption through previous star-formation episodes or fast gas outflows ejecting the gas reservoir (Tacchella et al. 2016; Dekel et al. 2023; Ferrara 2024; Ferrara et al. 2024).

However, the dynamical mass estimates using the velocity dispersion of a line are notoriously uncertain, hence an accurate measurement of the dynamical mass with dynamical modelling is needed (Kohandel et al. 2019). In this Letter, we investigate the evidence for a velocity gradient using the ALMA observations of $[\text{O III}]\lambda 88 \mu\text{m}$, to improve the measurement of the dynamical mass of JADES-GS-z14-0 and investigate the assembly of rotating discs in the early Universe.

Throughout this work, we adopt a flat Λ CDM cosmology: H_0 : $67.4 \text{ km s}^{-1} \text{ Mpc}^{-1}$, $\Omega_m = 0.315$, and $\Omega_{\Lambda} = 0.685$ (Planck Collaboration et al. 2020). With this cosmology, $1''$ corresponds to 3.3 kpc at $z = 14.18$.

2 OBSERVATIONS AND DATA REDUCTION

In this work, we use ALMA band 6 observations of JADES-GS-z14-0 as part of 2023.A.00037.S programme (PI. Schouws), which used two spectral configurations to target the $[\text{O III}]\lambda 88 \mu\text{m}$ emission line. The total on-source integration time is 2.82 hours per spectral configuration. We used the calibrated visibilities downloaded from

the ALMA archive, only selecting spectral configuration covering the detected $[\text{O III}]\lambda 88 \mu\text{m}$ emission line at 223.524 GHz, same data reduction as Carniani et al. (2024b)

In order to image the calibrated visibilities we used the Common Astronomy Software Applications package (CASA; McMullin et al. 2007; CASA Team et al. 2022), specifically the task `tclean`. Carniani et al. (2024b) and Schouws et al. (2024) detected the emission line with 6.7σ . To optimize the spatial resolution of our observations while maintaining sufficient SNR, we adopted Briggs weighting with a robust parameter of 0.5 and hogbom deconvolver. We opted for a pixel scale of $0.1''$, and a channel width of 10 km s^{-1} to create the final datacubes. We cleaned the images down to 3σ level ($\text{rms} = 0.1 \text{ mJy/beam}$). The final data cube has a resolution with a beam of $0.6'' \times 0.8''$, compared to the deconvolved rest-frame UV half-light radius from NIRC*am* imaging of $0.079''$.

3 DETECTION AND MODELLING OF VELOCITY GRADIENT

3.1 Velocity gradient in $[\text{O III}]\lambda 88 \mu\text{m}$

To investigate the presence of any velocity gradient traced by the $[\text{O III}]\lambda 88 \mu\text{m}$ emission line, we fitted each pixel of the data cube within a radius of $<0.5''$ with a single Gaussian model, with centroid, velocity width and amplitude as free parameters. We fitted this model using python’s `lmfit`. To construct the final map we opted for a SNR cutoff of 3. We show the final velocity and FWHM maps of $[\text{O III}]\lambda 88 \mu\text{m}$ in the top and middle left panels of Figure 1. The velocity map shows a velocity gradient in the northeast direction with velocities from $+40$ to -20 km s^{-1} . We verified this velocity gradient using three separate methods: 1) extracting integrated spectra from grid of apertures; 2) performing spectro-astrometry in the image plane; and 3) performing spectro-astrometry in the uv -plane.

To confirm the velocity gradient, we extracted the regional spectra from 3×3 square grid centred on the JADES-GS-z14-0. Each region has a size of $0.3'' \times 0.3''$ and we show these spectra on the right side of Figure 1. We fitted the extracted spectra using a single Gaussian profile to determine the velocity centroid of the emission line profile. The extracted spectra confirm the presence of the velocity gradient in JADES-GS-z14-0 along the north-east direction with maximum velocity difference between two regions of $42 \pm 14 \text{ km s}^{-1}$, a 3.0σ detection of the velocity gradient in JADES-GS-z14-0.

We further confirmed this velocity gradient using spectro-astrometry in both image and uv -plane. For the image plane analysis, we created two moment-0 maps of the $[\text{O III}]\lambda 88 \mu\text{m}$ emission line in the range $[0, 50] \text{ km s}^{-1}$ and $[-50, 0] \text{ km s}^{-1}$ to map of the redshifted and blueshifted parts of the emission line, respectively. These are shown as red and blue contours, respectively, on the moment-0 map in the bottom left panel of Figure 1. We measure the spatial offset between the red and blue centroids of $0.3 \pm 0.06''$, corresponding to $0.99 \pm 0.2 \text{ kpc}$.

We adopted a spectro-astrometry test in the uv -plane by performing a 2D Gaussian fitting to the uv -visibilities. We first extracted the uv -visibilities from the measurement set using spectral channels 66–70 for the blue side and channels 70–74 for the red side of the emission line. We fitted the model using MCMC fitting routine (`emcee`; Foreman-Mackey et al. 2013) and we plot the final posterior distribution of the offsets between the location of the red and blue side of the emission line and the centre of the galaxy in Figure 2. The final estimated distance between the red and blue sides is $0.28 \pm 0.10''$ ($0.92 \pm 0.33 \text{ kpc}$), clearly confirming the velocity gradient observed

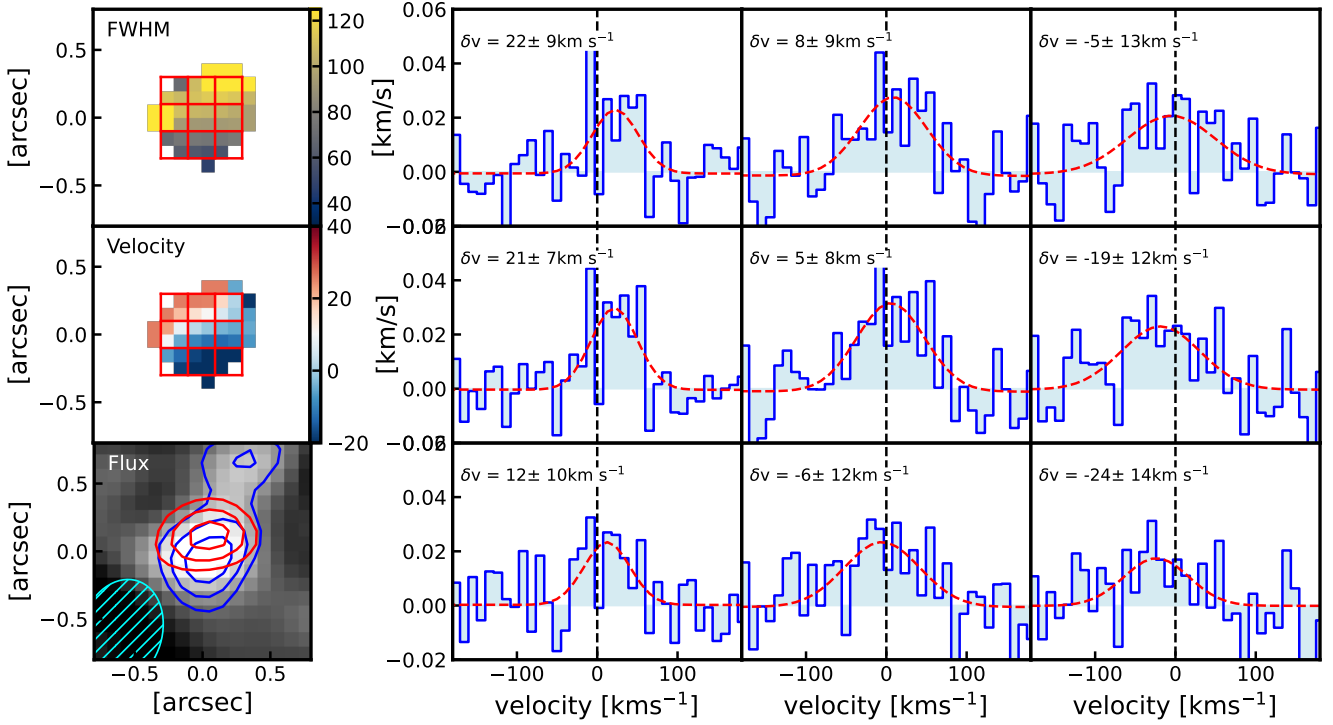


Figure 1. Tentative detection of the velocity gradient in JADES-GS-z14-0. Left top and middle panels: FWHM and velocity maps of the $[\text{O III}]\lambda 88\mu\text{m}$ emission line from Gaussian fitting. The red squares indicate the apertures used to extract spectra on the right. Bottom left: Moment-0 map extracted from $\pm 90 \text{ km s}^{-1}$. The red and blue contours show moment-0 maps extracted from $[-50, 0] \text{ km s}^{-1}$ and $[0, 50] \text{ km s}^{-1}$. The cyan-hatched ellipse shows the ALMA beam size. We observe $0.3 \pm 0.06''$ offset between the red and blue centroids. Right panels: $[\text{O III}]\lambda 88\mu\text{m}$ extracted from the square apertures indicated on velocity and FWHM maps. The data and the best-fit model are shown as blue and red lines. The extracted spectra confirm the derived velocity maps.

in the image plane. Furthermore, we split the observations into two exposures (1.4 hours on source per exposure) and confirmed our findings in both exposures. Overall, all three approaches show tentative evidence for a velocity gradient in JADES-GS-z14-0.

3.2 Modelling of the velocity gradient

In this section, we model the tentative velocity gradient detected in the previous section. Interpreting velocity gradients in low-resolution observations is challenging as mergers are often misinterpreted as rotating discs (e.g., Rizzo et al. 2022; Kohandel et al. 2020; Scholtz et al. 2024; Parlanti et al. 2024). However, in the NIRCcam images we do not see evidence of companions, double nuclei, tidal tails or any other complex structure usually associated to merger events. The presence of an outflow causing the observed gradient is also excluded based on the low velocity dispersion of the observations. We do not either see clear traces of streams of inflowing gas that could lead to kinematic distortions and dynamical instabilities like those observed in other high- z systems (e.g. SPT0311-58; Arribas et al. 2023). The measured offset of the red and blue centroids of $[\text{O III}]\lambda 88\mu\text{m}$ spectrum is also well above the diffraction limit of JWST at $3 \mu\text{m}$ ($0.1''$), implying that any companion or tidal tails above this spatial scale would have been detected in the NIRCcam images. Therefore, we will model this data by assuming it is a rotating disc.

We use the same method as described in Parlanti et al. (2023), using the publicly available Python library KINMS (Davis et al. 2020). Here we briefly describe the procedure. This method creates a mock data cube of a rotating disc based on the input parameters, convolves

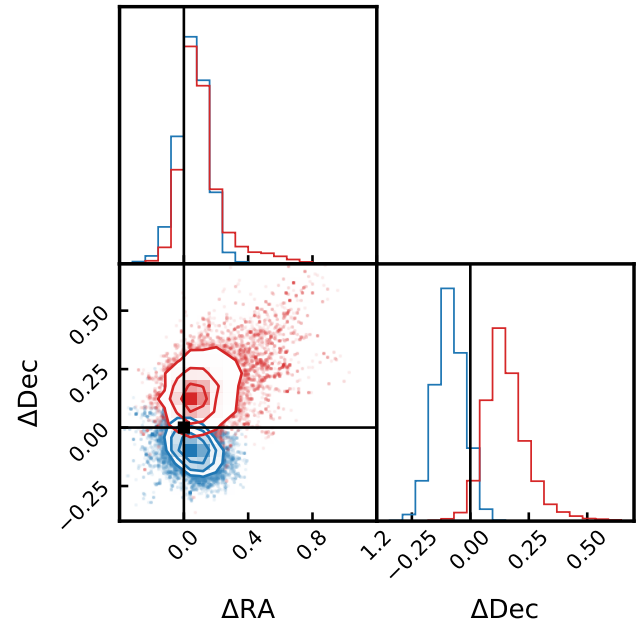


Figure 2. Spectro-astrometric analysis in the uv-plane. We show the posterior distribution of the spatial offset of the red and blue sides of the emission line from the centre of JADES-GS-z14-0. We see a spatial offset between the red and blue parts of the emission line, confirming the presence of the velocity gradient.

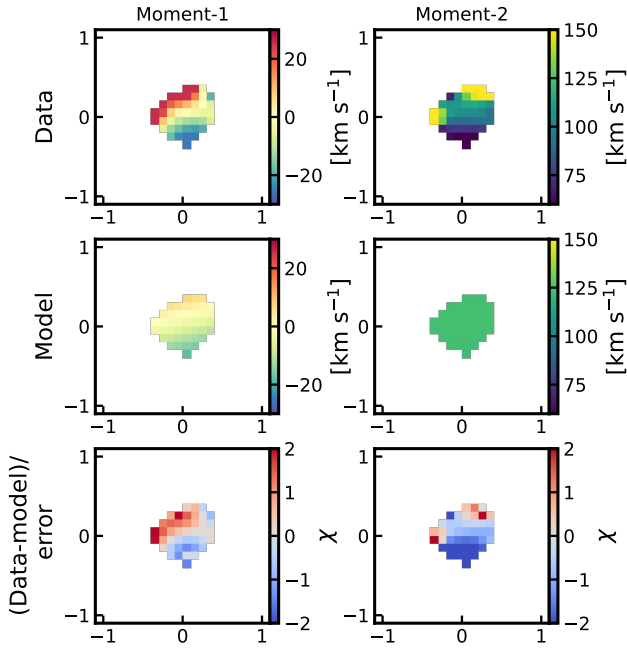


Figure 3. Moment maps created from the observed data (top row), maps from the best fit kinematical model of KinMS (centre row), and the normalised residuals (bottom row). The left and right columns show moment-1 and moment-2 maps.

it to match the spatial resolution of the observation to account for the beam-smearing effect, and then creates the model moment maps that we can directly compare with a set of observed ones. We set up KinMS to simulate the ALMA observations, with a spectral resolution of 10 km s^{-1} and angular resolution set to the beam size of our observations ($0.6'' \times 0.8''$ with an angle of 89°). To model the galaxy we assume that the matter is distributed in a thin exponential disc (Freeman 1970) with an intrinsic constant velocity dispersion profile. We set a uniform prior on the σ_v between 0 – 200 km s^{-1} . Using this setup we generate a mock cube and moment maps which are compared to the observed ones. The best-fit parameters are estimated using the package EMCEE (Foreman-Mackey et al. 2013). We used uniform priors on the inclination between 5° and 85° , and uniform priors on position angle between 0° and 180° . The dynamical mass was left free to vary with log uniform priors between 10^8 and $10^{11} M_\odot$ and we assumed uniform priors on the velocity dispersion between 5 and 200 km s^{-1} . We masked the pixels in the Moment-2 map with $\text{FWHM} > 150 \text{ km s}^{-1}$ as they are dominated by noise on the outskirts of the galaxy.

We fitted simultaneously the velocity and velocity dispersion maps derived in § 3.1 to estimate the inclination of the disc, dynamical mass, position angle, and intrinsic velocity dispersion (i.e. deconvolved by the instrumental spatial resolution), while we fixed the disc effective radius to the one found in Carniani et al. (2024a) from NIRCcam imaging of 260 pc (0.079 arcsec). We note that the stellar and ionised gas sizes were found to be comparable in the IFU observations (e.g. Förster Schreiber et al. 2018; Scholtz et al. 2018).

We show the comparison of the data and the fitted model in Figure 3. We note that the model is not fully able to reproduce the observed velocity gradient, due to the low value of the observed velocity dispersion. To reproduce the observed velocity gradient, the beam-smearing effect does increase the observed velocity dispersion. Modelling only the velocity gradient would improve the

fit of the velocity map and result in a higher dynamical mass, but would overestimate the observed velocity dispersion map. In this work, we used the approach of fitting the maps simultaneously. With low-resolution data, the beam-smearing effect causes the observed velocity dispersion to be affected by the underneath velocity gradient, adding little constraint to the overall fit. Higher-resolution observations would decrease the level of beam-smearing, allowing for a more accurate modelling.

Due to the low resolution of the data, we cannot simultaneously obtain tight constraints on the inclination and the dynamical mass of the system as they are degenerate (in low-resolution observations, models with constant $M_{\text{dyn}} \sin^2(\text{inc})$ are similar, see Figure A1). Due to the shape of the degeneration, even when the inclination is unconstrained, we are able to estimate, with large uncertainties, the dynamical mass of the system, obtaining a value of $\log(M_{\text{dyn}}/M_\odot) = 9.4^{+0.8}_{-0.4}$. Assuming that the mass is distributed as an exponential disc with the fixed effective radius of 260 pc and the dynamical mass obtained by the kinematic modelling, we computed the rotational velocity as the maximum velocity of the rotating disc occurring at $2.2 r_d \sim 340 \text{ pc}$. With these assumptions, we obtain an estimate of the rotational velocity of $V_{\text{rot}} = 164^{+248}_{-60} \text{ km s}^{-1}$. Interestingly we find a 3σ upper limit on the intrinsic velocity dispersion of $< 40 \text{ km s}^{-1}$ (3σ upper limit). This would result in an estimation of $V_{\text{rot}}/\sigma_v > 2.5$, which would imply tentative evidence for a kinematically cold disc in the first 300 Myr of the Universe’s lifetime. We compare our measurement of V_{rot}/σ_v with simulations and observations compiled from the literature by placing this estimate on a plot of V_{rot}/σ_v versus redshift (see Figure 4). We find that our measured tentative value for JADES-GS-z14-0 aligns with simulation predictions. It follows the evolutionary trend of $M_* > 10^9 M_\odot$ systems at $z > 6$. If confirmed, this would be the most distant dynamically settled disc structure observed to date.

Our measurement of M_{dyn} is consistent within 1σ with the values measured by Carniani et al. (2024b) and Schouws et al. (2024) from the velocity dispersion of the $[\text{O III}]\lambda 88\mu\text{m}$, but our errorbars fully capture the additional uncertainty due to the mass-inclination degeneracy. We derive a gas fraction of this galaxy of $60 \pm 20\%$, consistent with the value derived by previous analysis of the $[\text{O III}]\lambda 88\mu\text{m}$ observations of 36% (Schouws et al. 2024; Carniani et al. 2024b) and $< 70\%$ (Schouws et al. 2025). However, for better constraints on the kinematics of JADES-GS-z14-0, we would need higher sensitivity and resolution observations from ALMA or JWST/NIRSpec-IFS (see the results of our simulations in §4).

We also fitted the 1D velocity and velocity dispersion profiles, and the moment maps by using the dynamical fitting code DysmalPy (Price et al. 2021; Lee et al. 2024), which has proven to be a reliable method to recover the kinematical properties of datasets with low S/N and low spatial resolution. With this method, we obtain comparable results (within 1σ) for the dynamical mass and the velocity dispersion.

4 COMPARISON TO SERRA SIMULATIONS

We compare our results against mock $[\text{O III}]\lambda 88\mu\text{m}$ data generated from the SERRA suite of zoom-in, high-resolution cosmological simulations (Pallottini et al. 2022). These simulations achieve a mass resolution of $1.2 \times 10^4 M_\odot$, $\sim 25 \text{ pc}$ at $z = 7.7$, and incorporate non-equilibrium chemistry with on-the-fly radiative transfer. Their outputs are subsequently post-processed to generate FIR emission-lines (Pallottini et al. 2019) and hyperspectral datacubes (Kohandel et al. 2020), well-suited for producing realistic mock observations of the

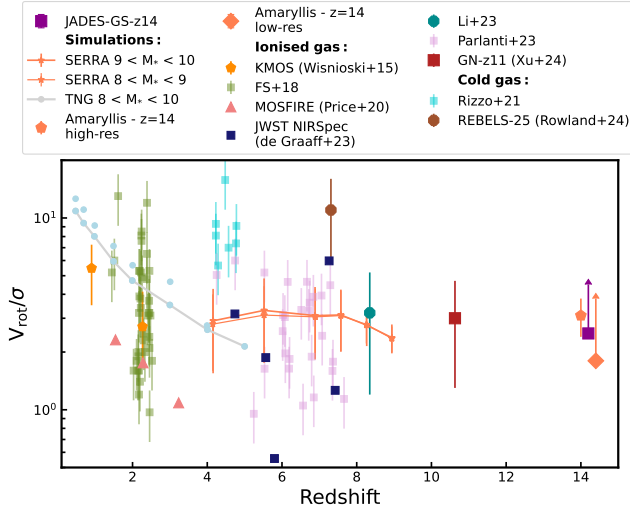


Figure 4. V_{rot}/σ_v versus redshift for observations and simulations. As we are unable to constrain the velocity dispersion of JADES-GS-z14-0 and in the low-resolution mock observations of Amaryllis from SERRA simulations, we only quote a lower limit on V_{rot}/σ_v for these. We compare JADES-GS-z14-0 to a compilation from the literature: *JWST*/NIRSpec, Illustris TNG (Pillepich et al. 2019), SERRA (Kohandel et al. 2024), ground-based IFU (Wisnioski et al. 2015; Förster Schreiber et al. 2018), MOSFIRE (Price et al. 2019), GN-z11 (Xu et al. 2024), ALMA z~6 (Parlanti et al. 2023), NIRSpec/MSA (de Graaff et al. 2024), ALMA z~4 (Rizzo et al. 2021), REBELS-25 (Rowland et al. 2024).

early Universe. In particular, we use the simulated galaxy “Amaryllis”, identified by Kohandel et al. (2023) as the brightest galaxy ($\log(L_{[\text{O III}]\lambda 88\mu\text{m}}/L_{\odot}) \approx 8.4$) in SERRA at $11 < z < 14$. Amaryllis has a stellar mass $\log(M_{\star}/M_{\odot}) \approx 8.8$ and $\text{SFR}_{10\text{Myr}} = 18 M_{\odot} \text{yr}^{-1}$, making it a close analogue to JADES-GS-z14-0. To generate synthetic ALMA observations, we select a viewing angle of 45° , at which the FWHM of the $[\text{O III}]\lambda 88\mu\text{m}$ emission line closely matched that of JADES-GS-z14-0. The effective radius of Amaryllis is ~ 180 pc, while JADES-GS-z14-0 has a size of 260 pc. To match this scale, we rescale the mock data by a factor of 1.5 to improve the comparison between the mock observations and JADES-GS-z14-0.

We used CASA’s `simobserve` with an array configuration of C5 and C7 corresponding to a resolution of $0.8''$ and $0.15''$, respectively. We use integration times of 2.85 and 10.0 hours for the C5 and c7 array configurations, respectively, to match the SNR of our current observations and of potential future deeper, higher-resolution ALMA and NIRSpec/IFS observations. We show the moment maps of Amaryllis (flux, velocity and FWHM) in Figure 5 for the low and high resolution observations.

The mock observations from the SERRA simulations in Figure 5 shows that a velocity gradient in a rotating galaxy at $z > 10$ like JADES-GS-z14-0 can be detected even in low-resolution observations (see top row of Figure 5). We modelled the mock observations using the same modelling setup described in § 3.2. Despite detecting the velocity gradient in the low resolution mock observations of Amaryllis simulations, we encountered similar degeneracies between inclination and dynamical mass as for the ALMA observations of JADES-GS-z14-0 and we can only estimate an upper limit to the velocity dispersion, therefore we are only able to estimate a lower limit on $V_{\text{rot}}/\sigma_v > 1.8$. However, using high spatial resolution observations ($\sim 0.15''$), which are achievable by both *JWST*/NIRSpec and ALMA observations, it would be possible to

resolve these high- z targets with more than three independent resolution elements (see beam size in Figure 5), which is the required condition to properly constrain a galaxy kinematics and distinguish rotating disks from close mergers (Rizzo et al. 2022). With such deeper high-resolution observations, it would be possible to break the degeneracy between the dynamical mass and inclination (see Figure A1 in Appendix, right panel) with a measured value of $V_{\text{rot}}/\sigma_v = 3.1 \pm 0.7$ and an uncertainty on the dynamical mass of 0.2 dex. This clearly shows that a follow-up with deep *JWST*/NIRSpec-IFS or ALMA observations is essential to constrain the kinematics of JADES-GS-z14-0.

5 CONCLUSIONS

In this letter, we re-examined the ALMA observations of $[\text{O III}]\lambda 88\mu\text{m}$ emission line in JADES-GS-z14-0 at $z \sim 14.2$, to constrain its kinematic properties. We created velocity maps, by fitting a Gaussian profile to $[\text{O III}]\lambda 88\mu\text{m}$ emission line, and we found evidence for a velocity gradient in the data with a maximum velocity difference of 50 km s^{-1} in the north-south direction. We confirmed the presence of the velocity gradient by 1) extracting regional spectra from 9 regions (see Figure 1); and 2) performing spectroastrometry in the image and uv planes, which found a spatial offset of $0.28 \pm 0.10''$ between the redshifted and blueshifted parts of the emission line (see Figures 1 and 2). Using these approaches we found similar velocity gradients.

Due to the lack of merger signatures and/or streams of gas associated to outflows and accretion of gas in the NIRCcam imaging, we modelled the galaxy kinematics assuming a thin rotating disc of size 260 pc. We measured a dynamical mass of $\log(M_{\text{dyn}}/M_{\odot}) = 9.4^{+0.8}_{-0.4}$. Our large uncertainties reflect the inability of the data with low spatial resolution to break the degeneracy between dynamical mass and inclination. However, our model fully captures this additional uncertainty, which is not accounted for by the virial estimator. We estimated a lower limit on the V_{rot}/σ_v of > 2.5 , which would indicate a settled dynamically cold at these high redshifts if confirmed.

We compared our observational results with mock observations from the SERRA cosmological simulations. We created mock ALMA $[\text{O III}]\lambda 88\mu\text{m}$ observations of an analogue of JADES-GS-z14-0 called “Amaryllis”, with both low and high spatial resolution setup ($0.8''$ and $0.15''$). We show that the tentative detection of the velocity gradient is possible even in the low-resolution data (see the top row of Figure 5). However, in order to break the degeneracy between dynamical mass and inclination, high spatial resolution observations ($< 0.2''$) are required. These high spatial resolution observations could confirm the high V_{rot}/σ_v in the galaxy and constrain the dynamical mass within 0.23 dex.

Our tentative detection of this velocity gradient suggests that the formation of early cold rotating structures in the Universe happened much sooner than previously anticipated in both observations and simulations. The discovery of a rotation-dominated disc just 300 Myr after the Big Bang would drastically change our view of early galaxies, and pose new challenges to the cosmological simulations, while putting constraints on feedback models. However, due to the limited resolution of the current observation we can only obtain a tentative detection of the presence of an early rotating disc. Further high spectral and higher spatial resolution deep observations with ALMA and *JWST* IFU are essential in order to resolve the kinematics of JADES-GS-z14-0 and investigate the formation of discs in the early Universe.

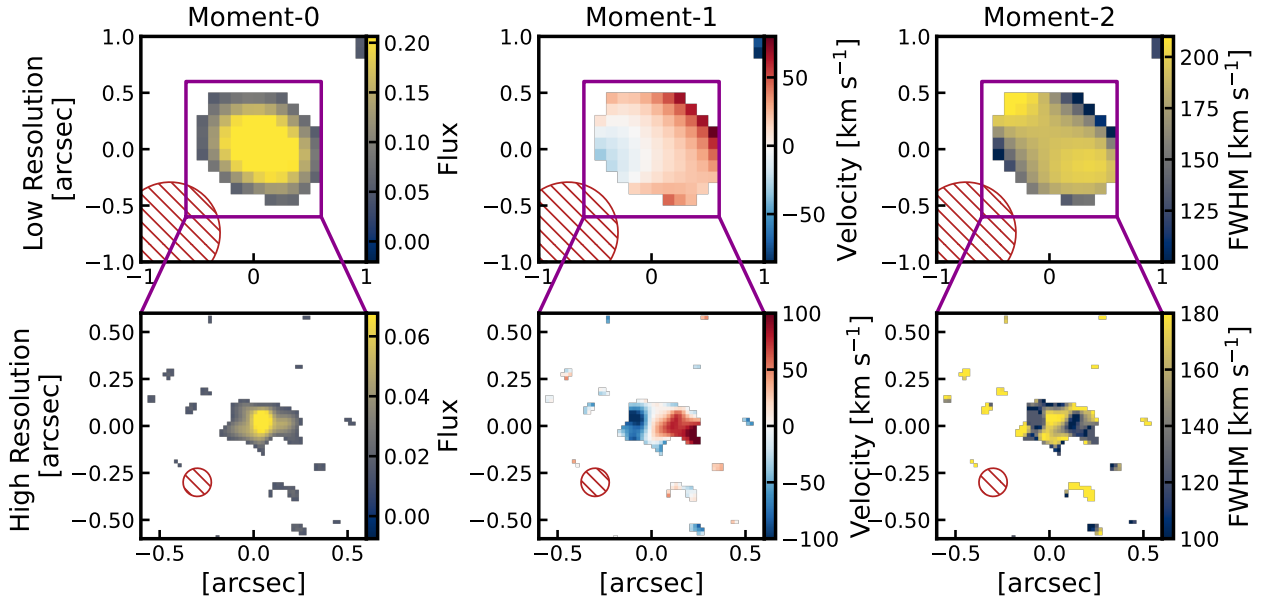


Figure 5. Mock observations of JADES-GS-z14-0 analogue in the SERRA simulations - "Amaryllis". The top row shows flux, velocity and FWHM maps of mock low-resolution ALMA observations (0.9''), while the bottom row shows mock high-resolution observations (0.15''). The simulations show that a rotating galaxy shows a small velocity gradient ($< 40 \text{ km s}^{-1}$) in the low-resolution data, similar to our observations. The simulations show that a rotating (thin) disc galaxy with a size and mass as JADES-GS-z14-0, and observed under similar conditions, should show a similar velocity gradient to the one obtained.

ACKNOWLEDGEMENTS

This paper makes use of the following ALMA data: ADS/JAO.ALMA#2023.A.00037.S ALMA is a partnership of ESO (representing its member states), NSF (USA) and NINS (Japan), together with NRC (Canada), MOST and ASIAA (Taiwan), and KASI (Republic of Korea), in cooperation with the Republic of Chile. The Joint ALMA Observatory is operated by ESO, AUI/NRAO and NAOJ. The National Radio Astronomy Observatory is a facility of the National Science Foundation operated under a cooperative agreement by Associated Universities, Inc. JS, FDE, RM and GCJ acknowledge support by the Science and Technology Facilities Council (STFC), ERC Advanced Grant 695671 "QUENCH" and the UKRI Frontier Research grant RISEandFALL. RM also acknowledges funding from a research professorship from the Royal Society. S.C, EP and GV acknowledge support from the European Union (ERC, WINGS,101040227) A.L.D. thanks the University of Cambridge Harding Distinguished Postgraduate Scholars Programme and Technology Facilities Council (STFC) Center for Doctoral Training (CDT) in Data intensive science at the University of Cambridge (STFC grant number 2742605) for a PhD studentship. SA acknowledges grant PID2021-127718NB-I00 funded by the Spanish Ministry of Science and Innovation/State Agency of Research (MICIN/AEI/ 10.13039/501100011033) AJB acknowledge funding from the "FirstGalaxies" Advanced Grant from the European Research Council (ERC) under the European Union's Horizon 2020 research and innovation programme (Grant agreement No. 789056). ZJ acknowledges JWST/NIRCam contract to the University of Arizona, NAS5-02015. BER acknowledges support from the NIRCam Science Team contract to the University of Arizona, NAS5-02015, and JWST Program 3215. We acknowledge the CINECA award under the ISCR initiative, for the availability of high performance computing resources and support from the Class B project SERRA HP10BPUZ8F (PI: Pallottini). We gratefully acknowledge the computational resources of the

Center for High Performance Computing (CHPC) at SNS. HÜ acknowledges support through the ERC Starting Grant 101164796 "APEX". IL acknowledges support from PID2022-140483NB-C22 funded by AEI 10.13039/501100011033 and BDC 20221289 funded by MCIN by the Recovery, Transformation and Resilience Plan from the Spanish State, and by NextGenerationEU from the European Union through the Recovery and Resilience Facility SA acknowledge grant PID2021-127718NB-I00 funded by the Spanish Ministry of Science and Innovation/State Agency of Research (MICIN/AEI/ 10.13039/501100011033)

DATA AVAILABILITY

The datasets were derived from sources in the public domain: ALMA data from https://almascience.nrao.edu/aq/?result_view=observation.

APPENDIX A: POSTERIOR DISTRIBUTION OF KINEMATICAL FITTING

We present the posterior distribution of our kinematical modelling of the ALMA data of JADES-GS-z14-0 and the mock observations of the galaxy Amaryllis from SERRA cosmological simulations (both low and high resolution) in Figure A1.

REFERENCES

- Abdurro'uf et al., 2024, *arXiv e-prints*, p. arXiv:2404.16201
- Arribas S., et al., 2023, *arXiv e-prints*, p. arXiv:2312.00899
- Bakx T. J. L. C., et al., 2021, *MNRAS*, 508, L58
- CASA Team et al., 2022, *PASP*, 134, 114501
- Cameron A. J., et al., 2023, *arXiv e-prints*, p. arXiv:2302.04298
- Carniani S., et al., 2024a, *arXiv e-prints*, p. arXiv:2405.18485

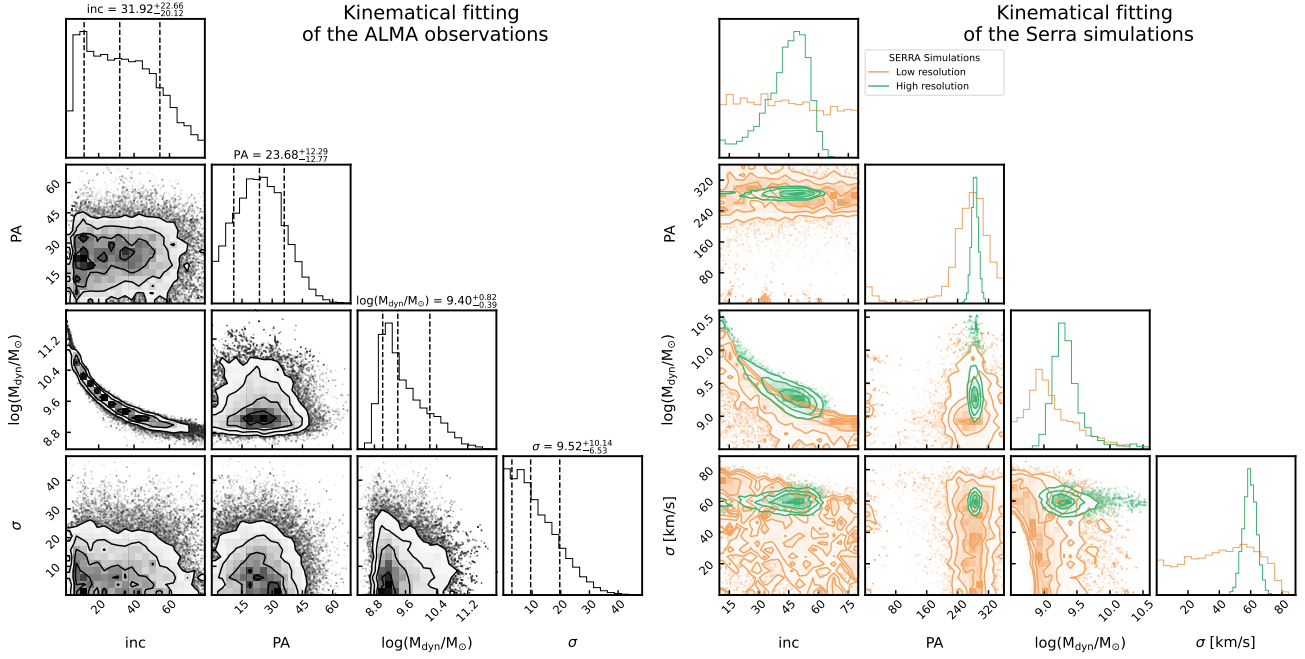


Figure A1. Posterior distribution from the kinematical modelling of ALMA data of JADES-GS-z14-0 (left panel) and mock observations of the galaxy Amariyllis from SERRA simulations (right panel).

Carniani S., et al., 2024b, [arXiv e-prints](#), p. [arXiv:2409.20533](#)

Chabrier G., 2003, [PASP](#), **115**, 763

Curtis-Lake E., et al., 2023, [Nature Astronomy](#), **7**, 622

Davis T. A., Zabel N., Dawson J. M., 2020, KinMS: Three-dimensional kinematic modeling of arbitrary gas distributions, Astrophysics Source Code Library, record ascl:2006.003

Dekel A., et al., 2009, [Nature](#), **457**, 451

Dekel A., Sarkar K. C., Birnboim Y., Mandelker N., Li Z., 2023, [MNRAS](#), **523**, 3201

Duan Q., et al., 2024, [arXiv e-prints](#), p. [arXiv:2407.09472](#)

Duncan K., et al., 2019, [ApJ](#), **876**, 110

Ferrara A., 2024, [A&A](#), **689**, A310

Ferrara A., Carniani S., di Mascia F., Bouwens R., Oesch P., Schouws S., 2024, [arXiv e-prints](#), p. [arXiv:2409.17223](#)

Foreman-Mackey D., Hogg D. W., Lang D., Goodman J., 2013, [PASP](#), **125**, 306

Förster Schreiber N. M., et al., 2018, [arXiv e-prints](#),

Fraternali F., Karim A., Magnelli B., Gómez-Guijarro C., Jiménez-Andrade E. F., Poses A. C., 2021, [A&A](#), **647**, A194

Freeman K. C., 1970, [ApJ](#), **160**, 811

Förster Schreiber N. M., et al., 2018, [ApJS](#), **238**, 21

Hainline K. N., et al., 2024, [arXiv e-prints](#), p. [arXiv:2404.04325](#)

Harikane Y., et al., 2023, [ApJS](#), **265**, 5

Harikane Y., et al., 2024, [arXiv e-prints](#), p. [arXiv:2406.18352](#)

Helton J. M., et al., 2024, [arXiv e-prints](#), p. [arXiv:2405.18462](#)

Hsiao T. Y.-Y., et al., 2023, [arXiv e-prints](#), p. [arXiv:2305.03042](#)

Inami H., et al., 2022, [MNRAS](#), **515**, 3126

Isobe Y., et al., 2023, [ApJ](#), **959**, 100

Jones G. C., et al., 2024, [arXiv e-prints](#), p. [arXiv:2405.12955](#)

Killi M., et al., 2023, [MNRAS](#), **521**, 2526

Kohandel M., Pallottini A., Ferrara A., Zanella A., Behrens C., Carniani S., Gallerani S., Vallini L., 2019, [MNRAS](#), **487**, 3007

Kohandel M., Pallottini A., Ferrara A., Carniani S., Gallerani S., Vallini L., Zanella A., Behrens C., 2020, [MNRAS](#), **499**, 1250

Kohandel M., Ferrara A., Pallottini A., Vallini L., Sommovigo L., Ziparo F., 2023, [MNRAS](#), **520**, L16

Kohandel M., Pallottini A., Ferrara A., Zanella A., Rizzo F., Carniani S., 2024, [A&A](#), **685**, A72

Krumholz M. R., Burkhard B., Forbes J. C., Crocker R. M., 2018, [MNRAS](#), **477**, 2716

Lamperti I., et al., 2024, [arXiv e-prints](#), p. [arXiv:2406.10348](#)

Larson R. L., et al., 2023, [arXiv e-prints](#), p. [arXiv:2303.08918](#)

Lee L. L., et al., 2024, [arXiv e-prints](#), p. [arXiv:2411.07312](#)

Lelli F., Di Teodoro E. M., Fraternali F., Man A. W. S., Zhang Z.-Y., De Breuck C., Davis T. A., Maiolino R., 2021, [Science](#), **371**, 713

Litke K. C., et al., 2023, [ApJ](#), **949**, 87

McMullin J. P., Waters B., Schiebel D., Young W., Golap K., 2007, in Shaw R. A., Hill F., Bell D. J., eds, *Astronomical Society of the Pacific Conference Series Vol. 376, Astronomical Data Analysis Software and Systems XVI*. p. 127

Neeleman M., Prochaska J. X., Kanekar N., Rafelski M., 2020, [Nature](#), **581**, 269

Orr M. E., et al., 2020, [MNRAS](#), **496**, 1620

Pallottini A., et al., 2019, [MNRAS](#), **487**, 1689

Pallottini A., et al., 2022, [MNRAS](#), **513**, 5621

Parlanti E., Carniani S., Pallottini A., Cignoni M., Cresci G., Kohandel M., Mannucci F., Marconi A., 2023, [A&A](#), **673**, A153

Parlanti E., et al., 2024, [arXiv e-prints](#), p. [arXiv:2407.19008](#)

Pillepich A., et al., 2019, [MNRAS](#), **490**, 3196

Planck Collaboration et al., 2020, [A&A](#), **641**, A6

Price S. H., et al., 2019, [arXiv e-prints](#)

Price S. H., et al., 2021, [ApJ](#), **922**, 143

Rizzo F., Vegetti S., Powell D., Fraternali F., McKean J. P., Stacey H. R., White S. D. M., 2020, [Nature](#), **584**, 201

Rizzo F., Vegetti S., Fraternali F., Stacey H. R., Powell D., 2021, [MNRAS](#), **507**, 3952

Rizzo F., Kohandel M., Pallottini A., Zanella A., Ferrara A., Vallini L., Toft S., 2022, [A&A](#), **667**, A5

Robertson B. E., et al., 2023, [Nature Astronomy](#), **7**, 611

Robertson B., et al., 2024, [ApJ](#), **970**, 31

Rowland L. E., et al., 2024, [arXiv e-prints](#), p. [arXiv:2405.06025](#)

Sanders R. L., Shapley A. E., Topping M. W., Reddy N. A., Brammer G. B., 2024, [ApJ](#), **962**, 24

Scholtz J., et al., 2018, [MNRAS](#), **475**, 1288

Scholtz J., et al., 2024, [arXiv e-prints](#), p. [arXiv:2411.07695](#)

Schouws S., et al., 2024, [arXiv e-prints](#), p. [arXiv:2409.20549](#)

- Schouws S., et al., 2025, *arXiv e-prints*, p. [arXiv:2502.01610](https://arxiv.org/abs/2502.01610)
Smit R., et al., 2018, *Nature*, 553, 178
Sommovigo L., et al., 2022, *MNRAS*, 513, 3122
Spilker J. S., et al., 2022, *ApJ*, 929, L3
Tacchella S., Dekel A., Carollo C. M., Ceverino D., DeGraf C., Lapiner S.,
Mandelker N., Primack Joel R., 2016, *MNRAS*, 457, 2790
Tacchella S., et al., 2023, *MNRAS*, 522, 6236
Tacchella S., et al., 2024, *arXiv e-prints*, p. [arXiv:2404.02194](https://arxiv.org/abs/2404.02194)
Tamura Y., et al., 2019, *ApJ*, 874, 27
Übler H., et al., 2024, *arXiv e-prints*, p. [arXiv:2403.03192](https://arxiv.org/abs/2403.03192)
Vikaeus A., et al., 2024, *MNRAS*, 529, 1299
Wisnioski E., et al., 2015, *ApJ*, 799, 209
Witstok J., et al., 2022, *MNRAS*, 515, 1751
Xu Y., et al., 2024, *ApJ*, 976, 142
de Graaff A., et al., 2024, *A&A*, 684, A87

This paper has been typeset from a $\text{\TeX}/\text{\LaTeX}$ file prepared by the author.